

Photoinduced reactions occurring on activated carbons. A combined photooxidation and ESR study

Leticia F. Velasco[†], Valter Maurino[‡], Enzo Laurenti[‡], Isabel M. Fonseca[§], Joao C. Lima[§], Conchi O. Ania^{†*}

[†] Dept. Chemical Processes in Energy and Environment, Instituto Nacional del Carbón, INCAR-CSIC, Apdo. 73, 33080 Oviedo, Spain.

[‡] Dip. di Chimica, Università di Torino, Via P. Giuria 5-7, 10125 Torino, Italy.

[§] REQUIMTE/CQFB, Dept. Química, Faculdade de Ciências e Tecnologia, Universidade Nova de Lisboa, 2829-516 Lisboa, Portugal.

*Corresponding author. Tel.: +34 985 118846; Fax: +34 985 297662. E-mail address: conchi.ania@incarcsic.es (CO Ania)

Keywords: hydroxyl radicals, ash-free materials, activated carbon, photooxidation, electron spin resonance

Abstract

This work demonstrates the ability of ash-free activated carbons to interact with UV light to promote the photooxidation of phenol in solution through the formation of radical species. Our results show that in the absence of inorganic impurities or semiconductor additives, the photodegradation efficiency of the studied activated carbons has to be ascribed to the carbon matrix itself. Hydroxyl radicals have been detected by spin trapping electron spin resonance spectroscopy upon UV irradiation of the activated carbon suspensions in aqueous solution. Although the ability to photogenerate radicals upon irradiation is well known in inorganic semiconductors (such as titanium dioxide) or carbon/semiconductor composites, we herein demonstrate the capacity of the carbon matrix alone to interact with UV light, generating reactive species that would be responsible for the observed photoinduced reaction using carbons alone in the absence of semiconductor additives. Thus, the conventional interpretation of the enhanced photodegradation efficiency of carbon/semiconductor photocatalysts -so far attributed to synergistic and confinement effects, and minimized surface recombination of the charge carriers- should be reconsidered to account for the radicals photogenerated when the carbons are exposed to UV light.

1. Introduction

The use of light energy has been long explored in environmental chemistry since the excitation of electronic molecular states at energies provided by light -typically corresponding to the UV region- may induce chemical bond breaking [1,2]. Heterogeneous photocatalysis based on semiconductors is becoming one of the most promising green chemistry technologies in the environmental remediation arena. Indeed, after the pioneering studies in 1977 reporting the ability of titania powders to decompose cyanides in solutions [3], the interest of semiconductor photocatalysis for environmental applications has become one of the most popular and promising Advanced Oxidation Process (AOP), particularly for the degradation of recalcitrant pollutants in air, water and wastewater [2].

The success of semiconductor photocatalysis as an efficient environmental remediation tool is mainly related to the choice of the photoactive material and its performance and stability under illumination conditions. Commonly used photocatalysts are based on wide band n-type semiconductors, mostly TiO_2 and ZnO , as well as other transition metal oxides and sulfides (e.g. CdS , WO_3) [2,4]. The mechanism of light absorption in a wide band gap n-type semiconductor is based on the photogeneration of electron/hole pairs, charge separation and migration of the carriers to the semiconductor surface initiating a series of chain redox processes. The competition between the recombination of these photogenerated charge carriers and their ability to lead to subsequent chemical events -eventually involving other reactive species- usually determines the overall efficiency of the photocatalytic process [5].

Triggered by the low efficiency of most semiconductors -typically associated to high surface recombination rates of the charge carriers and poor efficiency under visible light-, the control over the photocatalysts structure (i.e., morphology, particle size, crystallinity) has received

increasing attention in an attempt to improve the photocatalytic activity of semiconductors. Among different approaches, the synthesis of hybrid catalysts by immobilization of the photoactive semiconductor on appropriate supports has emerged as an effective alternative to improve the photodegradation yields of the resulting composites [6-8]. In this regard, the potential role of carbon materials as additives and supports for the immobilization of semiconductors has recently attracted considerable attention because of the increased efficiencies reported for carbon/semiconductor composites on the photodegradation of a variety of pollutants both in liquid and gas phase [8,9 and references there in].

Although the exact role of carbon materials in the enhanced photocatalytic response of carbon/semiconductor composites has not yet been fully understood, it has been generally attributed to several factors including the visible light absorption ability of some composites, synergistic effects due to the confinement of the pollutant on the porosity of the carbon support, and/or strong interfacial electronic effects of certain carbon nanostructures [8-11].

More recently, we have reported the anomalous photochemical response of activated carbons under UV light [12,13]. Direct irradiation of activated carbons in the absence of other semiconductor additives showed relatively high efficiencies towards phenol photo-oxidation beyond the so-called synergistic effect due to adsorption on the porosity and the direct photolysis (non-catalyzed reaction). The origin of the ability of the activated carbons to photo-oxidize phenol has been rather controversial since it does not seem to be an intrinsic property of activated carbons [10,12], but rather dependent on the characteristics (composition and structure) of the carbon material itself. Providing direct experimental evidence on the photoinduced reactions occurring at the interface of porous carbons upon UV irradiation becomes rather complex due to the confinement of the target pollutant on the porosity of the carbons. Moreover,

the main issue of concern seems to be whether the carbon matrix is capable of interacting with the UV light and if it is possible to demonstrate it beyond any reasonable doubt.

Bearing this in mind, we have pursued in our attempt to explore the response of activated carbons under UV light and to discriminate if this is due to the carbon matrix itself or to combined effects due to impurities (i.e., mineral matter) present in the activated carbon. To clarify this issue, an activated carbon with relatively large ash content was selected for this study and subjected to modifications to remove the inorganic impurities. The choice of the material was based on the anomalous photochemical response reported in previous studies towards phenol photooxidation in the absence of conventional semiconductors (i.e., titanium oxide) [12].

Although such ability of the pristine material to promote phenol photodegradation has been previously reported in aqueous medium [13], the outcome of the latter studies is used here for data interpretation so as to demonstrate the origin of such photochemical response when the carbon is exposed to UV light.

To avoid biased interpretations, certain experiments have been designed to eliminate the contributions of adsorption and photolysis to the overall photodegradation yield. This is important for porous materials as it becomes extremely difficult to discriminate between the contributions of the photooxidation reaction and the adsorption on the porosity, which occur simultaneously in these systems. Hence, we have also monitored the photooxidation of preadsorbed substrates. The obtained results provide experimental evidence on the photogeneration of radicals under UV illumination of semiconductor-free and ash-free carbon materials; this issue, long speculated in the literature is herein experimentally demonstrated by coupling photodegradation and spectroscopic measurements.

2. Experimental section

2.1 Materials

An activated carbon obtained by steam activation of bituminous coal was used (sample Q). To remove all the inorganic impurities (ash content) present on the pristine carbon an acid digestion treatment (HF/HCl) was carried out following the method proposed by Korver [14]. Briefly, about 10 g of the pristine carbon were introduced in a PTFE vessel and sequentially immersed in 100 mL of the following acids: HCl 5M, HF 40% and HCl 35%; the suspension was covered with a PTFE plate and heated at 55-60 °C (2° C/min) under continuous mild agitation and maintained at this temperature for 6 hours. After cooling down at room temperature, the acid was removed and the sample was rinsed in water and initiated the digestion with the following acid. The de-ashed carbon was labeled as QD. A second sample (labeled as QnoFe) was prepared by selectively removing the iron from the inorganic matter of the pristine carbon by digestion in 1.2 M HCl during 150 min at 60 °C (ratio 5 g carbon in 250 mL acid solution). The modified carbons were washed in hot water in a Soxhlet apparatus until constant pH.

2.2 Photooxidation tests

2.2.1 Photooxidation studies on preloaded carbons

For the evaluation of the photoresponse of the carbons eliminating the contribution of adsorption on the porosity, the carbon samples were previously loaded with phenol. About 40 mg of carbon were put in contact with a diluted phenol solution (i.e., 60 ppm) and allowed to equilibrate until all phenol was adsorbed in the carbon porosity and thus was no longer detected in solution. Then the carbon/water suspensions were irradiated at different times using a low pressure mercury lamp (6 W) in a “frozen-merry-go-round” geometry (i.e., several test tubes

disposed at fixed positions in a circular geometry around the lamp). The fixed positions are necessary since the test tubes have to be efficiently stirred during the illumination. The lamp is characterized by a 254 nm line and the photon flux ranged between $2.3\text{--}4.2 \times 10^{-7}$ einstein/s L for the different fixed positions. After irradiation, the solution was removed and the carbon phase was extracted in ethanol (i.e. 10 mL). The alcoholic solvent (ethanol) was chosen as it does not dissolve anything from the carbons alone and it has high solubility and extraction yields for phenol and its degradation intermediates (previously determined for each pure compound in all the carbons following a similar pre-adsorption procedure). Both the alcoholic extracts and the aqueous solutions were filtered using a 0.45 μm pore size cellulose acetate filter previous analysis; phenol and its degradation intermediates were analyzed by reverse phase HPLC (Spherisorb C18 column (125 mm x 4 mm), methanol-water mixture (5:95), photodiode array detector). All the experiments were done in triplicate and demonstrated to be reproducible with less than 5 % deviation; reported data represent the average values. The blank reaction under UV light and in the absence of photoactive material (photolysis) was carried out as reference.

2.2.2 Photodegradation efficiency in aqueous solution

Phenol photooxidation was also evaluated from aqueous solution in a batch photoreactor, as described elsewhere [12]. Briefly, photodegradation kinetics were measured for 6 hours for all the samples, and small aliquots of the solution (~ 0.5 mL) were taken out at regular time intervals and analyzed by reverse-phase HPLC. Total Organic Carbon (TOC) content of the solution after 6 hours of irradiation was also analyzed.

2.3 Materials characterization

2.3.1 N₂ adsorption

Textural characterization of the carbons was carried out by measuring the N₂ adsorption isotherms at -196 °C in an automatic apparatus (Micrometrics ASAP 2020). Before the experiments, the samples were outgassed under primary vacuum at 120 °C overnight. The isotherms were used to calculate specific surface area S_{BET} , total pore volume V_{T} (evaluated at relative pressure p/p° of 0.99) and micro/mesopore volumes using the NL-DFT method assuming a slit-shape pore geometry.

2.3.2 SEM measurements

SEM analyses were performed with a FE-SEM apparatus (QuantaSEM, FEI). Dispersion of the mineral impurities present on the carbon was analyzed by energy dispersive X-rays (EDX) spectroscopy. No metallic coating was required for the observation of the activated carbon.

2.3.4 Atomic Absorption Spectrometry

The contents of major and trace elements in the mineral matter of the pristine carbon were determined by Atomic Absorption Spectrometry (AAS) in a Shimadzu AA-6300 apparatus. The carbon matrix was removed by calcination and the obtained ashes were previously dissolved by alkaline fusion using boric acid and lithium carbonate in a muffle furnace at 1000°C for 3 h in air atmosphere. The melted materials were cooled to room temperature and brought into solution using a mixture of inorganic acids (4N HNO₃ and concentrated HCl). The resulting acidic solutions were analyzed by AAS for trace elements determination.

2.3.5 X-ray diffraction

XRD patterns were recorded on a Bruker D8 Advance instrument operating at 40kV and 40 mA and using CuK α ($\lambda = 0.15406$ nm) radiation. Diffraction data were collected by step scanning with a step size of $0.02^\circ 2\theta$ and a scan step time of 2 s.

2.3.6 Electron Spin Resonance (ESR)

DMPO (5,5-dimethyl-N-oxide pyrrolidone) was used as trapping agent of radicals. About 0.5 g/L of the carbon samples were suspended in 5 ml of HClO₄ buffer (pH 3), and the appropriate volume of DMPO was added to the suspension to reach a final concentration of 18 mM. Samples were introduced in capillary quartz cells and irradiated for 5, 10, 20, 45 and 60 minutes. ESR spectra were immediately recorded from the solution (after filtering out the solids) at room temperature on a Bruker ESP 300E X band spectrometer with the following spectral parameters: receiver gain 10^5 ; modulation amplitude 0.52 G; modulation frequency 9.69 GHz; conversion time 40.96 ms; microwave power 5.024 mW; center field 3450 mT, sweep width 120 mT. Simulations of the individual components of the ESR spectra were obtained using the Winsim 2002 software [15].

3. Results and discussion

3.1 Characteristics of the studied materials

The main characteristics of the pristine and modified activated carbons about porosity and surface chemistry are summarized in Table 1. To facilitate a direct comparison of the samples and the evaluation of the de-ashing treatment on the chemical composition of the carbons, raw data are presented in Table 1 (rather than the usual normalization on a dry ash free basis). Data indicate that the acid digestions did not modify either the textural features of the raw material

(i.e., similar surface areas and microporosity) or the chemical composition, beyond the complete removal of the mineral matter. It can also be observed that there was not incorporation of other heteroatoms (i.e., oxygen, nitrogen) to the carbon matrix during the de-ashing treatments; the slight decrease in the pH_{PZC} of both QnoFe and QD materials (Table 1) is attributed to the acidification of the samples due to the severe acid digestions, and not to the incorporation of new surface groups in the carbons.

An important characteristic of the pristine carbon is its large ash content, which composition and surface distribution was analyzed by AAS and SEM (Figure 1). Typical EDX spectra representative of the distribution of the major constituents of the inorganic impurities on the carbon matrix are given in Figure 1. Major elements in the pristine carbon were silicon, oxygen and aluminium, with traces of iron (ca. accounting for about 1 wt.% in the overall carbon composition upon quantification by AAS). After the treatment in 1.2 M HCl, the traces of iron were selectively removed (sample QnoFe), whereas consecutive digestion steps in HF/HCl caused the complete elimination of the mineral matter of the carbon (sample QD), as inferred by the chemical composition in Table 1. The XRD patterns of the carbons shown in Figure 1 also confirmed this observation; the sharp peaks characteristic of silica (quartz phase) in sample Q disappeared after the treatment in HF/HCl. However, all the carbons showed the broad peaks at 25° and 44° , corresponding to the (002) and (100) reflections characteristic of amorphous carbons.

3.2 Phenol photodegradation from solution

The photooxidation performance of the prepared carbons towards phenol degradation was initially evaluated from aqueous solution. The corresponding yields, in terms of phenol

disappearance both in dark conditions and under UV irradiation are shown in Table 2 and Figure 2. Phenol removal by adsorption was rather similar in all three studied carbons, which was somehow expected considering their similarities in texture and composition (Table 1). Slight differences in the adsorption kinetics are evident at short times, which are attributed to the slow phenol adsorption kinetics under acidic conditions [16]. However, the amount adsorbed at dark conditions after 6 hours is similar for all three studied materials (Table 2), as it was also confirmed by the similar Total Organic Carbon (TOC) values (ca. 15-18 mg C/L for Q, QnoFe and QD).

Under UV irradiation, both the rate and the amount of phenol disappearance increased significantly for the studied carbons, with respect to dark adsorption (Figure 2). Moreover, TOC values also decreased under irradiation, with values going down to 10-15 mg C/L for the carbons (the highest value corresponded to QD). Although in these tests various phenomena occur simultaneously (i.e., adsorption and photodegradation) [13], what is importantly observed here is the correlation of the photochemical performance with the inorganic impurities present on the carbons.

First of all, similar degradation kinetics were obtained for samples Q and QnoFe under UV light; given the similar porous and chemical features of both carbons (Table 1), these results indicate that the iron species present on this carbon matrix do not contribute to its photoactivity (despite iron is known to be active in fenton-like reactions). On the other hand, phenol conversion under UV light decreased upon the complete removal of the inorganic impurities (sample QD), pointing out the important role of the mineral matter on the photochemical behaviour of this material. However, still phenol removal efficiency obtained after the complete demineralization of the carbon was higher than that obtained upon adsorption (Figure 2), pointing out a

contribution of the carbon matrix in the absence of inorganic impurities in the photochemical response of the material. Analysis of the photooxidation intermediates detected in solution also showed the preferential formation of catechol in the presence of the carbon materials [9,11].

It is important to consider that a fraction of the intermediates will be adsorbed in the porous network of the carbons; hence to counteract the adsorption process and to discriminate the conversion due to photodegradation reactions, a series of experiments were carried out on carbons preloaded with phenol. This experimental systematic allows to eliminate the contributions of adsorption and photolysis, and thus to isolate the effect of the carbon matrix and the impurities on the ability of these materials to promote photooxidation of phenol [13].

3.3 Photoactivity of preloaded samples

As above-mentioned, the iron species present on the mineral matter of the pristine carbon appeared to be non-photoactive under UV light, as samples QnoFe and Q showed similar results in terms of phenol conversion from solution (Table 2 and Figure 2). Thus, irradiation of preloaded carbons was explored on carbons Q and QD, so as to evaluate the effect of the carbon matrix and the inorganic impurities. Preloading of the carbons was carried out using a low phenol concentration (see experimental section) so as to avoid irreversible adsorption of the pollutant inside the porosity of the carbons [16]; otherwise, the fraction of phenol molecules irreversibly adsorbed would not be extracted, and this would prevent the quantification of phenol and degradation intermediates retained inside the carbons.

Neither phenol itself nor any other compound were detected in the aqueous solution after irradiation of the preloaded carbons, which confirms that none of these compounds are released (desorbed) to the solution during the irradiation of the preloaded carbons. This is important since

it allows to disregard any contribution of photolysis during these assays, and confirms that the photoinduced reaction (if any) necessarily occurs inside the carbon phase and should thus be analyzed from the extracts.

Figure 3 A shows the evolution of phenol degradation versus the irradiation time for the preadsorbed carbons, evaluated from the alcoholic extracts. Data corresponding to the direct photolysis in solution (absence of photoactive material) are also plotted for comparison. Phenol degradation increased with the irradiation time for both activated carbons; this clearly demonstrates that a photoinduced reaction takes place inside these carbon matrices when exposed to UV light. Comparatively, although phenol conversion decreased after the complete removal of the inorganic impurities of the pristine carbon, for both activated carbons the photo-oxidation yield in terms of phenol conversion was higher than that obtained for the photolytic reaction (ca. 38 and 16 % for Q and QD, respectively, vs 4% for photolysis after 2.5 hours of irradiation). Moreover, this conversion corresponds to the ability of the carbons to degrade the phenol molecules adsorbed inside the porous structure, which is lower for carbon QD but not negligible. Indeed, considering the light absorption and scattering properties of activated carbon particles, it seems reasonable that the actual incident photon flux reaching the adsorbed molecules inside the porosity of the carbon will be much lower than the photon flux provided by the lamp and also than the flux capable of promoting the direct photolysis (when phenol molecules are in solution). Despite of this, the photoconversion of phenol was found to be higher for the preloaded carbons than in solution. All this corroborates the outstanding role of the ash-free carbon matrix on the photodegradation process.

The decrease in the photoresponse of the de-ashed carbon, compared to the pristine material, demonstrates that the inorganic matrix of this sample is also responsible for its photochemical

behavior. However, sample QD still showed quite relevant photoactivity, showing that the photoactivity is also somehow linked to the carbon matrix itself since this material has no inorganic impurities (removed completely during the demineralization treatment). These results are in good agreement with the photooxidation performance observed in solution (Figure 2) and with previous investigations reporting the photochemical response of several activated carbons under UV light [12].

Since the selective removal of the iron content of the mineral matter (sample QnoFe) revealed that the iron species of this material are not photoactive (Figure 2) -and thus fenton-like reaction are discarded in these systems-, the origin of the photochemical response of the mineral matter in carbon Q should be linked to the major components other than iron (see Figure 1). Further studies are currently ongoing to understand the role of the ashes based on their composition.

It is also interesting to point out that the rate of phenol conversion inside the carbons (in terms of mol degraded per time, Figure 3A) is quite fast for both activated carbons after short irradiation times, following a smoother pattern at longer times as the amount of phenol is reduced. This suggests that the efficiency of any carbon-mediated photoinduced reactions likely arising at the carbon surface upon UV irradiation is very high, readily leading to phenol oxidation. Although the mechanism for the carbon/UV light interactions still remains uncertain, it seems that the location of phenol molecules inside the porosity of the carbons somehow has a positive effect on the efficiency of the photoinduced reaction. If photogenerated species are likely to be formed upon irradiation of the carbons, then the proximity of the target pollutant to the photoactive centers or reactive species created upon irradiation of the carbon would increase the probability of substrate reaction. In contrast, for direct photolysis the amount of degraded phenol followed a linear dependency with the irradiation time, although the values were much

smaller than those obtained upon irradiation of the loaded carbons (ca. between 10 and 5 times lower than Q and QD, respectively).

The concentration of intermediates detected inside the carbon matrix (analyzed from the alcoholic extracts) also varied with time, showing a different trend for both carbons (Figures 3B and 4). In the case of carbon Q there is a gradual decrease in the amount of intermediates with the irradiation time, which suggests that, along with phenol, this carbon is capable of promoting the photooxidation of the intermediates. This is important for achieving high overall process efficiencies. Indeed, Figure 4 shows the speciation of the intermediates detected in the extracts with catechol, quinones and resorcinol as main subproducts. It has to be reminded that for the experiments carried out in the preloaded carbons no compounds were detected in the aqueous solution at any time.

What is interestingly inferred from Figure 4 is that the relative abundance of the degradation intermediates was rather similar for the preloaded carbons (qualitatively) with catechol as main intermediate. Even though the overall photooxidation yield decreased after removal of the ash content of the pristine carbon, a similar phenol photodegradation pathway (via catechol formation) [17] seems to apply for both carbons (compared to that of photolysis). Conversely, large differences were noticeable compared to photolysis where the amounts of catechol and quinones (hydroquinone and benzoquinone) were similar, suggesting the lack of a preferential oxidation route via catechol. The modification of phenol photodegradation pathway when using carbon materials as additives to inorganic semiconductors (typically TiO_2) has already been described in the literature [11].

3.3 ESR study

To further explore the mechanism of the photoinduced reactions occurring at the carbon surface when exposed to UV irradiation, ESR measurements were carried out for the activated carbons aiming at investigating the formation of paramagnetic species (i.e., radicals) during irradiation, as support of the information obtained by the photodegradation studies -both in solution and on the preloaded carbons-.

The formation of radical species was detected by a nitron spin trapping agent (5,5-dimethylpyrroline N-oxide, DMPO). This compound is capable of forming spin adducts with hydroxyl and superoxide radicals, creating more stable nitron radicals, easily detected by ESR spectroscopy [18,19]. Figure 5 shows the ESR spectra obtained for the DMPO adduct during UV irradiation of the activated carbons. Data corresponding to TiO₂ powders (Evonik, P25) are also included for comparison purposes. It should also be pointed out that no ESR signals were observed when DMPO alone was irradiated from the aqueous solution (in the absence of photoactive materials) or when the measurements were performed in dark conditions.

The ESR spectra of the carbon samples showed a quartet line profile with a 1:2:2:1 intensity pattern, and at $g = 2.006$ with $a_N = a_{H\beta} = 14.8$ G hyperfine splitting constants. This is consistent with the spectra reported in the literature for the DMPO-OH adduct [19] and confirms the formation of •OH radicals during the irradiation of both carbons. Simulation of the experimental spectra allowed the identification of additional adducts, less intense, for the titanium oxide (see triangles in Figure 4). Based on the simulated hyperfine splitting constants (Table 3) these were identified as HDMPO-OH, which is also originated upon reaction of DMPO with hydroxyl radicals [20].

The intensity of the ESR signals reached a maximum at 20 min (see example for Q carbon in the inset in Figure 5A). Due to the overall poor signal/noise ratio, quantitative analysis was

performed over the intensity of the line showing the highest signal/noise ratio, for an irradiation time fixed at 20 min. The amount of •OH radicals formed during the irradiation of Q and QnoFe (i.e., 0.29, 0.34 μM , respectively) was similar than for TiO_2 (i.e., 0.24 μM) under the same experimental conditions. This is in good agreement with the similar photoactivity detected for both carbons in aqueous solution.

In the case of sample QD, quantification was not possible due to the high noise to signal ratio, although the formation of •OH radicals is still evident. A tentative approximation could be done considering that the intensity of the signal decreased by almost 3 times (with respect to the pristine carbon). This provides a direct experimental evidence of the ability of the ash-free carbon matrix to interaction with UV light to photogenerated radical species that would be later used in the photooxidation of phenol.

It is also interesting to remark that the shape of the ESR spectra is similar to that obtained for conventional semiconductors (i.e., titanium oxide) reported in the literature [21]. Although the photogeneration of radical species has long been reported for semiconductors, and long speculated for carbon/semiconductor composites, we herein provide an experimental evidence of their formation. Moreover, the intensity of the signals corresponding to Q and QnoFe samples was similar to that obtained for the titania powders; in this regard, considering the porous nature of the studied carbons it is likely that a fraction of the DMPO spin adducts could be trapped inside the porosity of the carbons, rather than diffusing towards the bulk solution (where they are measured). Thus, the actual concentration of radical species could be higher than that measured from the solution.

The ESR signals for the spin adducts DMPO-OOH and/or DMPO-O₂ have also been reported in the literature [19,22], although these two adducts were not detected for the studied carbons;

this was somewhat expected considering that superoxide radical anions are rather unstable in water medium (the solvent here employed in the ESR measurements) and that the kinetics of the reactions between $\bullet\text{OOH}/\bullet\text{O}_2^-$ and DMPO are typically much slower than the formation of DMPO-OH spin adduct [22-24]. However, it has been reported that superoxide anions (if formed) are rapidly degraded to $\bullet\text{OH}$ radical and could eventually contribute to the DMPO-OH adduct signal [25]. Thus the occurrence of superoxide radical cannot be completely discarded by ESR; besides it is rather suspected as the overall degradation yield was reduced when the experiments were carried out under similar conditions in oxygen-free atmosphere (between 7-8 %).

The formation of $\bullet\text{OH}$ radicals seems reasonable since water is the reaction medium during the illumination of the carbons. Furthermore, $\bullet\text{OH}$ radicals might also be formed inside the carbon matrix, which would explain the experimentally observed photodegradation of the phenol preadsorbed inside the carbon matrix. This is supported by the fact that water molecules are co-entrapped in the carbon porosity upon immersion in the aqueous solution and associated to the target pollutant during the adsorption process [16]. Consequently the photogenerated radicals inside the carbon would be more easily transferred to the adsorbed phenol molecules, accounting of the experimentally observed photodegradation. Indeed, it is well known that hydroxyl radicals are extremely powerful oxidants with redox potential (i.e., $E^0 = +2.80 \text{ V}$ vs Normal Hydrogen Electrode) high enough to oxidize aromatic pollutants [26].

Summarizing, our results demonstrate that semiconductor-free activated carbons are capable of photogenerating reactive species - $\bullet\text{OH}$ radicals- under UV light, that can effectively react with aromatic compounds promoting their oxidation. Although the formation of $\bullet\text{OH}$ radicals has long been reported for carbon/semiconductor composites [27], our results demonstrate the formation

of radicals upon irradiation of carbon materials in the absence of impurities associated to the ashes (demineralized carbons) or any other semiconductor additives as titanium oxide, zinc oxide, etc.

The basis of the carbon-light interactions are unfortunately not fully understood, although they could be linked to the occurrence of electronic transitions at defective graphene layers of the carbon matrix upon light absorption. The photoinduced excited electronic state created at the reactive sites (defects and/or vacancies) of the carbon would easily undergo rapid charge transfer reactions -i.e., water photooxidation- to generate radicals, or other redox reactions involving the carbon matrix itself and/or phenol and its degradation intermediates. Such transitions have been postulated to apply in the photoluminescence of carbon nanostructures [28], the photoreduction of dissolved O₂ at irradiated highly oriented pyrolytic graphites [29], and the increased photocurrents measured upon irradiation of carbon/semiconductor photoelectrodes [30]. On the other hand, the photogeneration of charge carriers upon UV illumination has also been reported for certain carbon nanostructures such as carbon nanotubes [31].

These findings also point out that a new insight must to be considered to explain the enhanced photoconversion yields of carbon/semiconductor composites traditionally ascribed to confinement effects and minimized surface recombination in semiconductors [8,9]. Direct interaction of the carbon matrix with the UV light must be considered, given the ability of certain carbon matrices to absorb photons generating unstable electronic states that lead to hydroxyl radicals and therefore promote the oxidation of recalcitrant pollutants. This ability of activated carbons to generate reactive species upon UV irradiation offers new perspectives for carbon materials and opens the door to explore innovative applications related with solar energy conversion and AOP applied to environmental remediation.

4. Conclusions

Our results have confirmed the ability of ash-free and semiconductor-free activated carbons to absorb photons and generate •OH radicals when exposed to UV irradiation in aqueous medium. Furthermore, preliminary data has disclosed the capacity of activated carbons to generate a similar or even higher quantity of hydroxyl radicals than commercial titania powders. These findings constitute a first step towards the understanding of the origin of the photochemical response showed by certain semiconductor-free activated carbons under UV irradiation. Heretofore, activated carbons have been mainly used as non-photoactive supports of semiconductors in the photodegradation of pollutants.

The formation of spin adducts of reactive oxygen species, herein detected by ESR confirmed that UV irradiation of certain activated carbons can start the oxidation of preadsorbed organic substrates. These results are very interesting, in as much as activated carbon is the most widely used adsorbent for wastewater remediation based on adsorption technology. We believe this provides new perspectives and very useful information from the viewpoint of the design of low-cost and more efficient photoactive materials for environmental remediation. It also opens the door to explore innovative applications of carbon materials, such as photo-assisted regeneration of exhausted carbons, or photoelectrochemical applications (i.e., solar energy conversion).

Acknowledgments

This work is supported by the Spanish MINECO (grants CTM2008/01956, CTM2011/23378 and AIB2010PT-00209) and PCTI Asturias (grant PC10-002). L.F. Velasco thanks CSIC for her JAE-Pre contract.

References

- [1] R.P. Wayne, Principles and applications of photochemistry, second ed., Oxford Science Publications, Oxford University Press, USA, 1988.
- [2] N. Serpone, E. Pelizzetti (Eds), Photocatalysis: fundamental and applications, Wiley Interscience, New York, 1989.
- [3] S. N. Frank, A.J. Bard, J. Phys. Chem. 81 (1977) 1484-1488.
- [4] A.L. Linsebigler, L. Guangquan, J.T. Yate, Chem. Rev. 95 (1995) 735-758.
- [5] N. Serpone, D. Lawless, R. Khairutdinov, E. Pelizzetti, J. Phys.Chem. 99 (1995) 16655-16661.
- [6] M.A. Henderson, Surf. Sci. Reports 66 (2011) 185-297.
- [7] A. Fernández, G. Lassaletta, V.M. Jiménez, A. Justo, A.R. González-Elipe, J.M. Herrmann, H. Tahiri, Y. Ait-Ichou, Appl. Catal. B Environ. 7 (1995) 49-63.
- [8] R. Leary, A. Westwood, Carbon 49 (2011) 741-772.
- [9] J.L. Faria, W.H. Wang, in P.h. Serp, J.L. Figueiredo (Eds.), Carbon Materials for Catalysis, Wiley & Sons, New Jersey, 2009, pp. 481-506.
- [10] J. Matos, J.M. Herrmann, Appl. Catal. B Environ. 18 (1998) 281-291.
- [11] J. Araña, J.M. Doña-Rodríguez, E. Tello Rendón, C. Garriga i Cabo, O. González-Díaz, J.A. Herrera-Melián, J. Pérez-Peña, G. Colón, J.A. Navío, Appl. Catal. B Environ. 44 (2003) 153-160.
- [12] L.F. Velasco, I.M. Fonseca, J.B. Parra, J.C. Lima, C.O. Ania, Carbon 50 (2012) 249-258.
- [13] L.F. Velasco, J.B. Parra, C.O. Ania Appl. Surf. Sci. 256 (2010) 5254-5258.
- [14] J.A. Korver, Chemical Weekblad 46 (1950) 301-302.
- [15] D.R. Duling, J. Magn. Res. Series B 104 (1994) 105-110.

- [16] L.F. Velasco, C.O. Ania, *Int. J. Adsorpt.* 17 (2011) 247-254.
- [17] A. Santos, P. Yustos, A. Quintanilla, S. Rodríguez, F. García-Ochoa, *Appl. Catal. B Environ.* 39 (2002) 97-113.
- [18] E.G. Janzen, B.J. Blackburn, *J. Am. Chem. Soc.* 91 (1969) 4481-4490.
- [19] E. Finkelstein, G.M. Rosen, E. Rauckman, *J. Arch. Biochem. Biophys.* 200 (1980) 1-16.
- [20] K. Makino, A. Hagi A, H. Ide, A. Murakami, M. Nishi, *Can. J Chem.* 70 (1992) 2818-2827.
- [21] M.A. Grela, M.E.J. Coronel, A.J. Colussi, *J. Phys. Chem.* 100 (1996) 16940-16946.
- [22] C. Chen, X. Li, W. Ma, J. Zhao, H. Hidaka, N. Serpone, *J. Phys. Chem. B* 106 (2002) 318-324.
- [23] S. Horikoshi, H. Hidaka, N. Serpone, *J. Photochem. Photobiol. A: Chem.* 153 (2002) 185-189.
- [24] J. Zhao, T. Wu, K. Wu, K. Oikawa, H. Hidaka, N. Serpone, *Environ. Sci. Technol.* 32 (1998) 2394-2400.
- [25] B. Gray, A.J. Carmichael, *Biochem. J.* 281 (1992) 795-802.
- [26] P.M. Wood, *Biochem. J.* 253 (1988) 287-289.
- [27] Y. Yu, J.C. Yu, C.-Y. Chan, Y.-K. Che, J.-C. Zhao, L. Ding, W.-K. Ge, P.-K. Wong, *App. Catal. B Environ.* 61 (2005) 1-11.
- [28] Q. Bao, J. Zhang, C. Pan, J. Li, C. Li, J. Zang D.Y. Tang, *J. Phys. Chem. C*, 111 (2007) 10347-10352.
- [29] A.D. Modestov, J. Gun, O. Lev, *Surf. Sci.* 417 (1998) 311-322.
- [30] M. Haro, L.F. Velasco, C.O. Ania, *Catal. Sci. Technol.* 2 (212) 2264-2272.
10.1039/c2cy20270k.

[31] S. Lu, B. Panchapakesan, *Nanotechnol.* 17 (2006) 1843-1850.

Table 1. Main textural and chemical characteristics of the studied activated carbons. To facilitate direct comparison of the samples, the raw chemical composition is presented (rather than normalized on a dry-ash free basis).

	Q	QD	QnoFe
S_{BET} [m²g⁻¹]	1033	1080	1032
V_{TOTAL} [cm³ g⁻¹]^a	0.52	0.53	0.52
V_{MICROPORES} [cm³ g⁻¹]^b	0.32	0.33	0.32
V_{MESOPORES} [cm³ g⁻¹]^b	0.09	0.08	0.08
C [wt.%]	85.5	96.5	87.2
H [wt.%]	0.4	0.6	0.5
N [wt.%]	0.5	0.7	0.6
O [wt.%]	1.9	1.9	1.9
S [wt.%]	0.3	0.3	0.3
Ash content [wt.%]	11.4	0.0	9.5
pH_{PZC}	9.1	7.6	7.4
^a evaluated at p/po 0.99			
^b evaluated by NLDFT applied to N ₂ adsorption data			

Table 2. Phenol disappearance (%) from aqueous solution under dark conditions and upon different times of UV irradiation for the studied carbons.

	UV light	
	6 hours	10 min
Q	98	66
QnoFe	99	51
QD	93	29
Dark conditions		
Q	80	42
QnoFe	81	40
QD	75	18

Table 3. ESR parameters of the DMPO adducts formed upon UV irradiation of Q, QnoFe, and QD: aN and aH (β , γ) are the nitrogen and hydrogen hyperfine splitting constants, respectively; % represents the partition coefficient of the detected adducts. For comparison purposes, the parameters corresponding to commercially available TiO₂ (Evonik, P25) are also included.

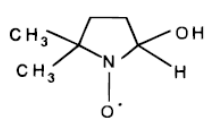
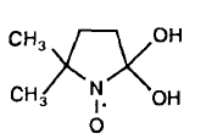
	 DMPO-OH			 HDMPO-OH		
	aN	aH(β)	%	aN	aH(γ)	%
Q	14.97	14.68	100	--	--	--
QD	14.98	14.68	100	--	--	--
QnoFe	14.97	14.68	100	--	--	--
TiO₂	14.95	14.67	80.3	14.86	1.01	19.7

Figure 1. (I) SEM image (top left) and EDX analysis of the main constituents of the ash content of the pristine activated carbon. (II) XRD patterns corresponding to both carbons and (III) relative abundance of the major elements in the mineral matter (wt. %).

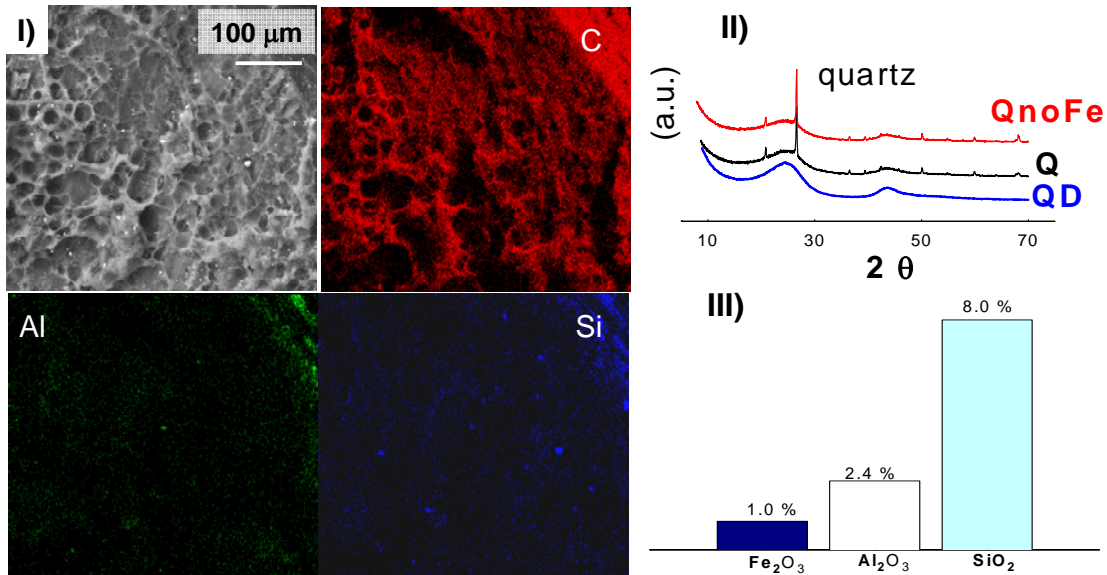


Figure 2. Evolution of phenol disappearance under dark conditions (A) and UV irradiation (B) in the studied materials from solution. The corresponding mols of the main intermediates detected in solution for each material are also shown: cathecol (triangles), hydroquinone (circles) and benzoquinone (squares).

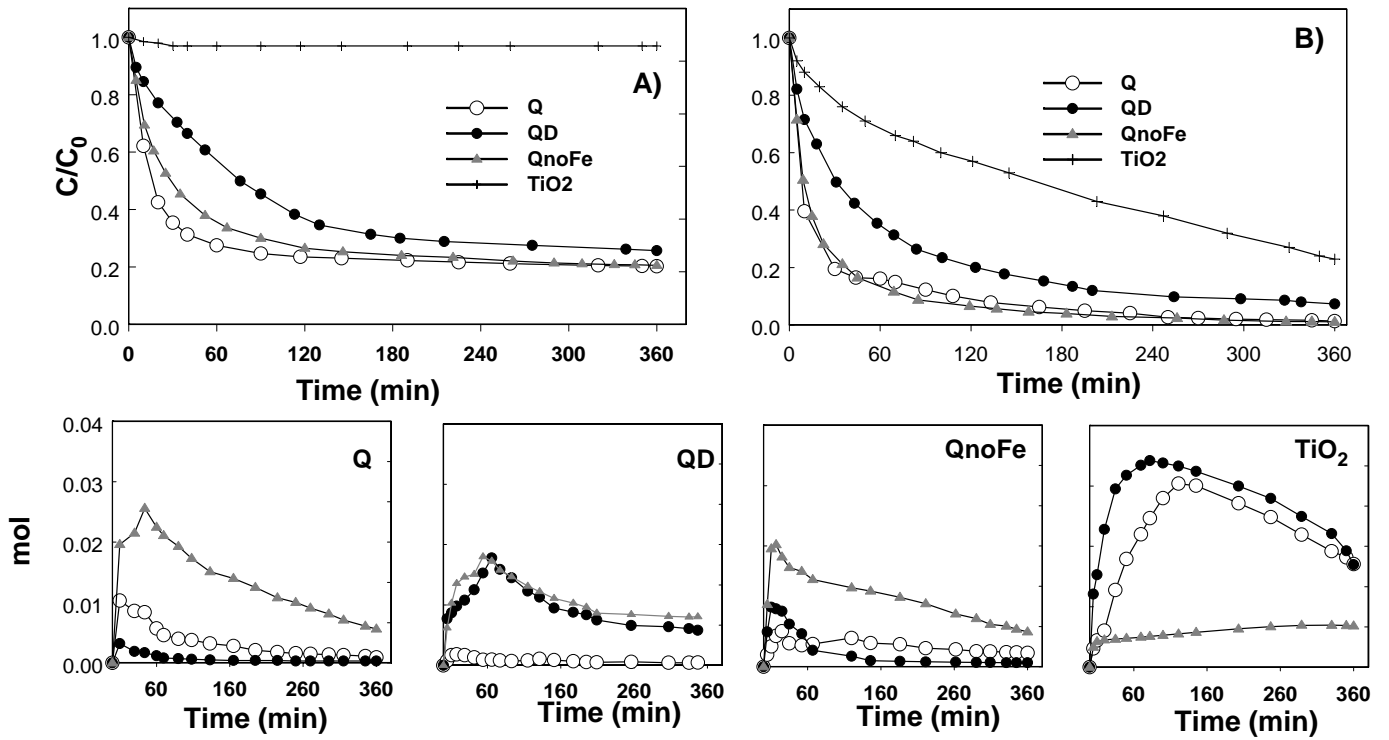


Figure 3. Evolution of phenol conversion inside carbon Q (black) and QD (striped) with the irradiation time in terms of (A) mols of degraded phenol and (B) mols of intermediates detected in the alcoholic extracts. Data corresponding to photolysis from solution are also included for comparison (grey).

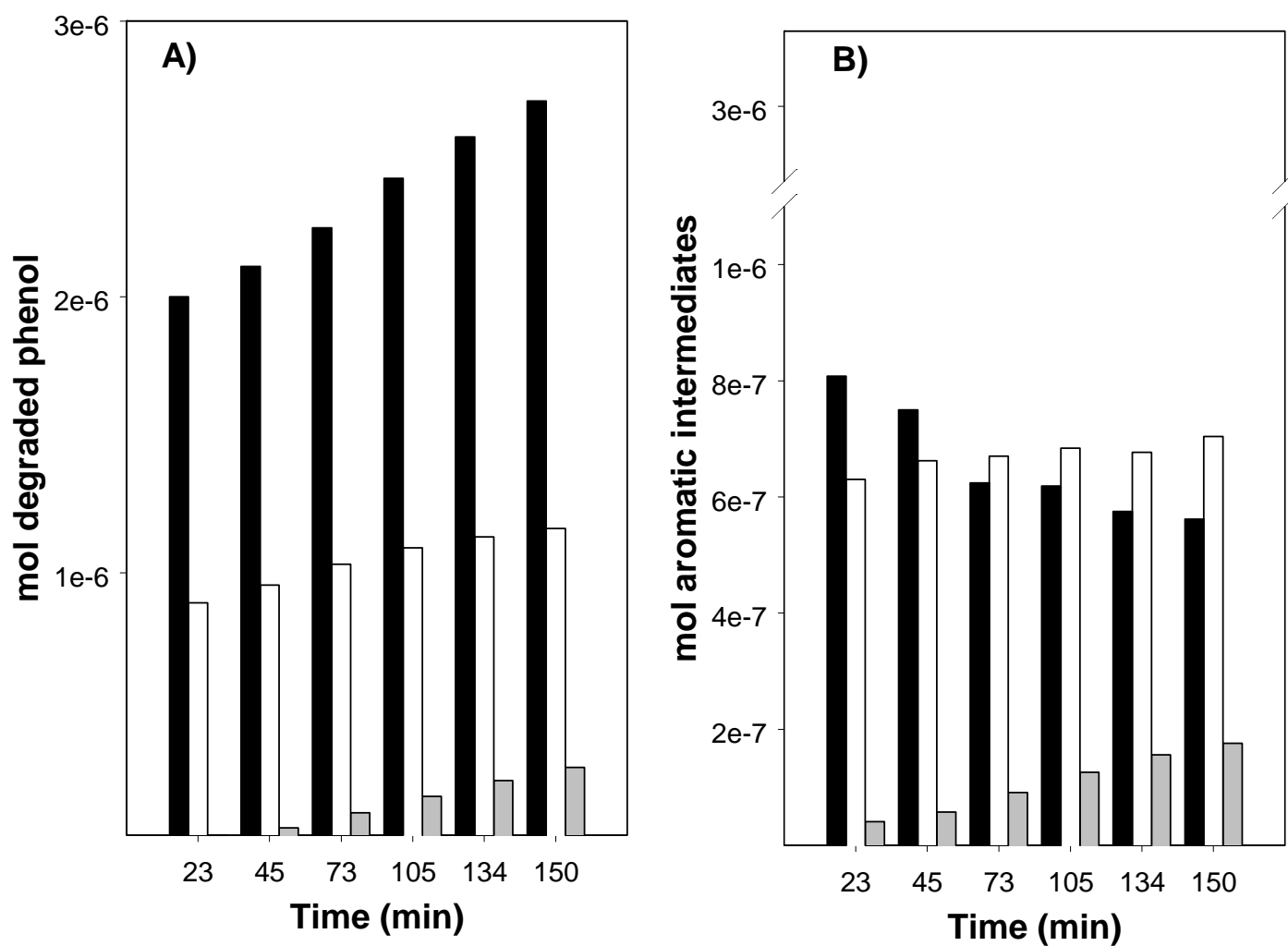


Figure 4. Speciation of phenol photooxidation intermediates detected in the alcoholic extracts after irradiation of the activated carbons. Solid squares (resorcinol), empty circles (benzoquinone), solid triangles (catechol), stars (hydroquinone). Data corresponding to photolysis from solution are also included as a comparison.

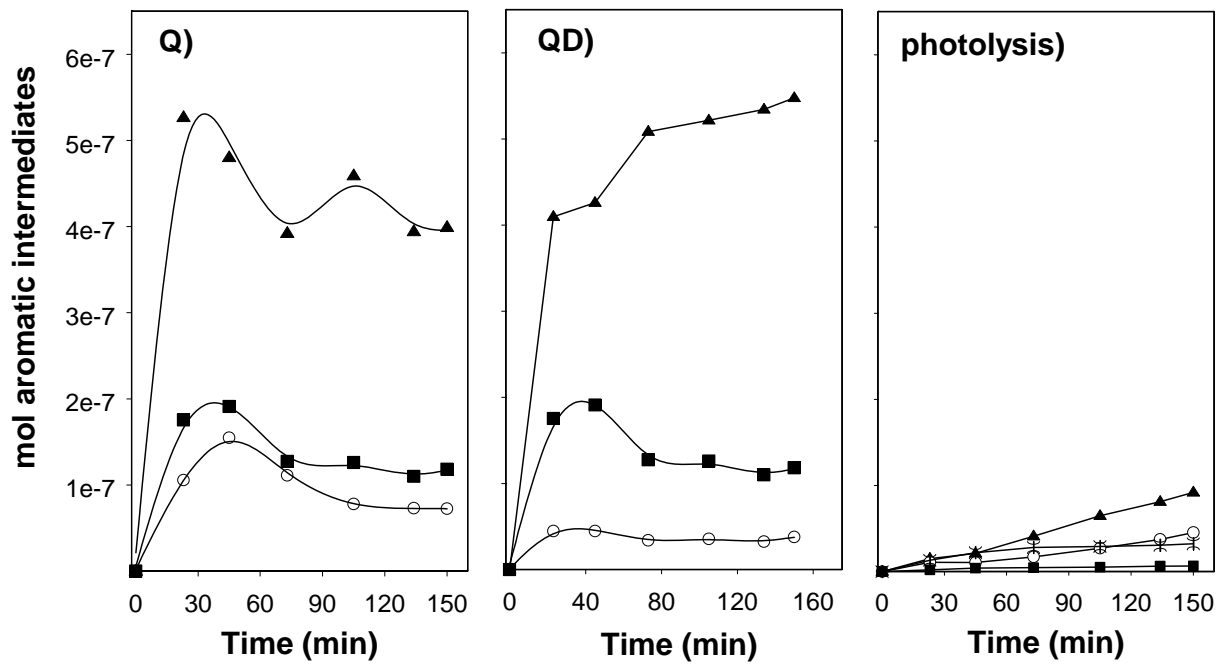
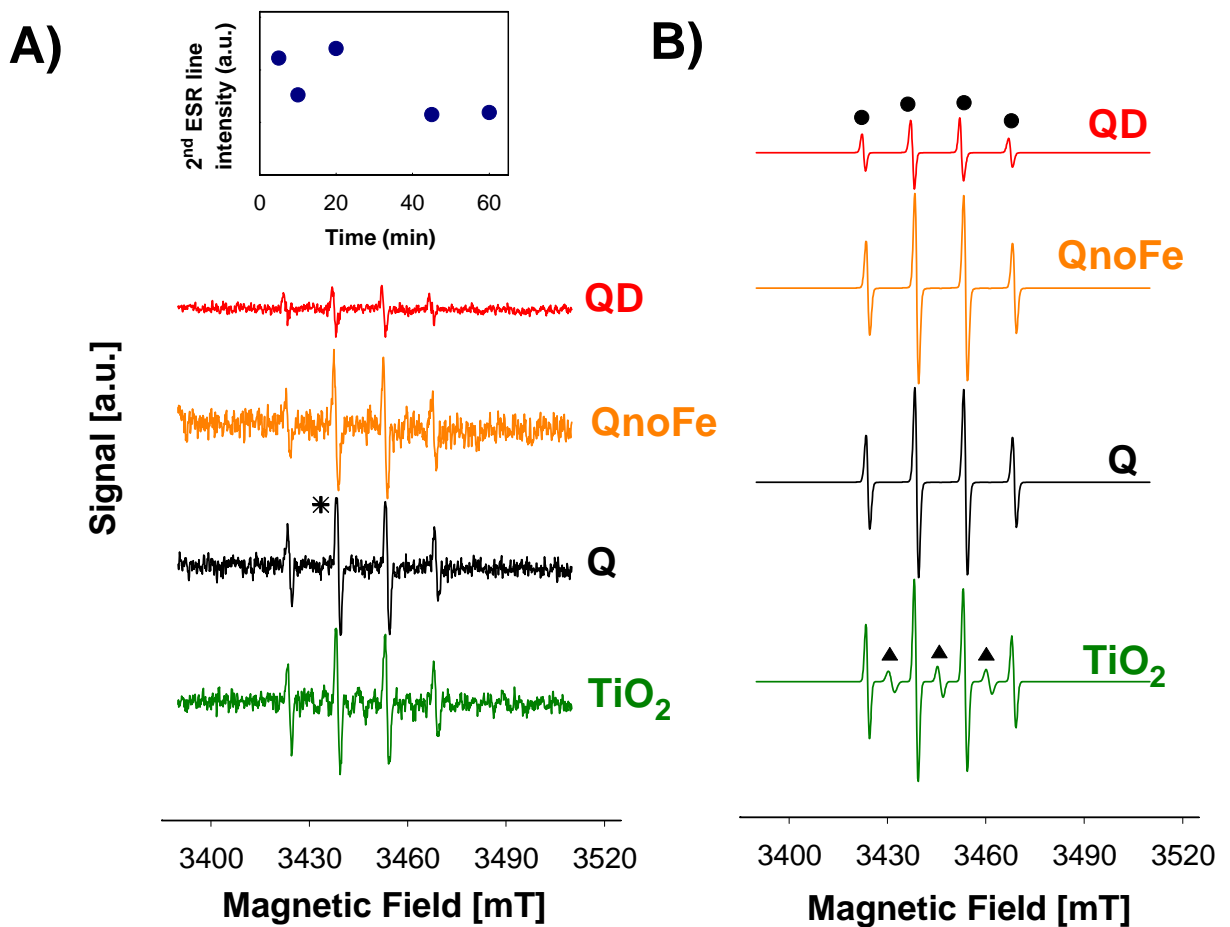


Figure 5. Experimental (A) and simulated (B) ESR spectra of the activated carbons Q, QnoFe, QD, and commercial TiO_2 powders. Assignments to DMPO-OH (circles) and HDMPO-OH (triangles) adducts are indicated. Inset: example of the evolution of the intensity of the second line of the ESR spectrum (*) with the irradiation time for sample Q.



Supplementary Data

Photoinduced reactions occurring on activated carbons. A combined photooxidation and ESR study

Leticia F. Velasco[†], Valter Maurino[‡], Enzo Laurenti[‡], Isabel M. Fonseca[§], Joao C. Lima[§], Conchi O. Ania^{†*}

[†] Dept. Chemical Processes in Energy and Environment, Instituto Nacional del Carbón, INCAR-CSIC, Apdo. 73, 33080 Oviedo, Spain.

[‡] Dip. di Chimica, Università di Torino, Via P. Giuria 5-7, 10125 Torino, Italy.

[§] REQUIMTE/CQFB, Dept. Química, Faculdade de Ciências e Tecnologia, Universidade Nova de Lisboa, 2829-516 Lisboa, Portugal.

*Corresponding author. Tel.: +34 985 118846; Fax: +34 985 297662. E-mail address: conchi.ania@incar.csic.es (CO Ania)

CONTENTS

Irradiation set-up **S1**

LIST OF FIGURES AND TABLES

Figure S1. Detail of the experimental setup for the irradiation of the samples: a) test tubes containing the phenol solution and/or the pre-adsorbed activated carbon; b) irradiation lamp; c) frozen merry-go-round support

S1. Irradiation set-up

A low pressure mercury lamp (6 W) was used to irradiate the samples in a “frozen-merry-go-round” geometry (Figure S2), i.e., several test tubes (typically 6) were disposed in a circular geometry around the lamp at fixed positions (not rotating as in the classical merry-go-round). The fixed positions are necessary since the test tubes have to be efficiently stirred in order to maximize the area of the activated carbon exposed to the UV light.

Prior to each experiment the photon flux arriving at each of the test tubes was measured through ferrioxalate actinometry (0.006 M) [H.K. Kuhn, H.K., S.E., Braslavsky, R. Schmidt, Chemical Actinometry (IUPAC Technical Report), Pure Appl. Chem., 76, 2105–2146, 2004.]. The quantum yield of phenol photolysis (ϕ) -defined as the ratio between the number of mol reacted, ΔN , and the mole of photons absorbed ($I_A \Delta t$)- was evaluated from the slope of the relation between the mol of pollutant degraded vs the irradiation time, using the equation:

$$\Delta N = \phi I_A \Delta t$$

where I_A is the photon flux absorbed by the sample, evaluated from the product of the incident photon flux I_0 , determined by actinometry, and the integrated absorption fraction F_S over the wavelength range used in the experiment:

$$I_A = I_0 F_S = I_0 \left(1 - 10^{-\bar{A}_T}\right) \frac{\varepsilon_f \bar{C}_f b}{\bar{A}_T} \Delta t$$

being A_T the total absorbance given by the compound and its degradation intermediates, ε_f phenol molar absorptivity coefficient, C_f the concentration of phenol, and b the light path in cm.

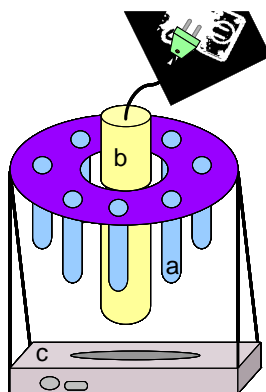


Figure S1. Detail of the experimental setup for the irradiation of the samples: a) test tubes containing the phenol solution and/or the pre-adsorbed activated carbon; b) irradiation lamp; c) frozen merry-go-round support.